Available online at www.sciencedirect.com

ScienceDirect

Procedia Engineering 197 (2017) 13 – 22

Procedia Engineering

www.elsevier.com/locate/procedia

DYMAT 23rd Technical Meeting

Dynamic Fracture of Ductile Materials

Deformation and Rupture of Armour Grade Steel Under Localised Blast Loading

B. McDonald[a,b,*], H. Bornstein[c], G. Langdon[d], R. Curry[d], A. Orifici[a]

[a]*School of Engineering, RMIT Universtiy, PO Box 71, Bundoora, Victoria 3083, Australia*
[b]*Defence Materials Technology Centre (DMTC), 24 Wakefield St, Hawthorn, Victoria 3122, Australia*
[c]*Defence Science and Technology Group (DST-G), 506 Lorimer St, Fishermans Bend, Victoria 3207, Australia*
[d]*BISRU, Department of Mechanical Engineering, University of Cape Town, Rondebosch 7700, South Africa*

Abstract

A series of 30 blast experiments were conducted on monolithic steel panels of two armour grade steels. The two steels evaluated were a high hardness armour (HHA) and a rolled homogenous armour (RHA). Tests were conducted at two standoff distances using a fixed charge diameter. The charge weight was varied to produce specific magnitudes of blast loading and to isolate the rupture threshold of each material. The results indicated that the HHA steel, generally reserved for ballistic protection, outperformed a more ductile RHA steel in terms of both its deformation resistance and rupture threshold. Optical and scanning electron microscopy was utilised for fractographic analysis of the ruptured plates. The failure of the steels in this investigation was found to be initiated by slant shear fracture with little to no localised thinning. This is in contrast to the tensile instability and ductile tearing predicted by established theories of plate rupture for mild steels under blast loading. The deformation and rupture of the candidate steels was analysed for all experimental conditions and compared to current empirical models based on a non-dimensional impulse parameter. While deformation behaviour is well predicted, the blast rupture threshold of the armour grade steels is poorly captured by current empirical modelling approaches. The identified shear fracture mode leads to lower energy absorption capabilities of the material compared to more ductile tensile failure.

Peer-review under responsibility of the scientific committee of the International Conference on Dynamic Fracture of Ductile Materials

Keywords: Armour Steel; Blast Loading; Shear Fracture

* Corresponding author. Tel.: +61 3 9629 8243; fax: +61 3 9626 8999.
E-mail address: brodie.mcdonald@dsto.defence.gov.com.au

Peer-review under responsibility of the scientific committee of the International Conference on Dynamic Fracture of Ductile Materials
doi:10.1016/j.proeng.2017.08.077

1. Introduction

The threat of improvised explosive devices (IED's) and landmines has resulted in the need to provide increased protection to armoured vehicles, without increasing the mass, to ensure adequate manoeuvrability is maintained [1]. One approach to address this requirement is the integration of high hardness armour (HHA) steels commonly reserved for ballistic protection applications into the lower-hull structure of an armoured vehicle.

HHA steel possesses a high yield strength which has been shown to improve deformation resistance under blast loading [2, 3, 4]. However, the performance of HHA steels in terms of their resistance to rupture has not been extensively studied. The limited ductility commonly associated with high yield strength steels may limit their protective capacity due to brittle fracture behaviour which is an issue that must be addressed before they can be integrated into an armour system.

Previous research on the fracture of locally blast loaded plates has generally focused on low strength structural materials. Nurick and Radford [5] examined the rupture of mild steel plates exposed to localised blast loading and identified several distinct damage modes with increasing magnitudes of blast loading. The initial damage mode of large inelastic deformation (Mode I) produced global deflection of the plate with a secondary bulge superimposed directly under the location of the explosive charge. With increased levels of blast loading, tensile instability leading to plate thinning and strain localisation was identified at the inflexion point of the central bulge and was termed Mode Itc. With adequate loading, partial and subsequently total tearing of the thinned region was observed (labelled Mode IIc* and Mode IIc respectively) ejecting the central disk of material from the plate with kinetic energy proportional to the overmatch of the blast loading [6]. At loading magnitudes beyond the rupture threshold, capping failure was followed by further cracking initiated from the central fracture surface and propagating radially. These cracks form several segments of material which continue to deform creating the characteristic shape of the final damage mode labelled petalling failure.

While the tensile damage mode observed at the transition from mode I to mode IIc has been observed in other studies [4, 6, 7] and has become established in theories of blast induced rupture, other research suggests that it may not be applicable to all steels or loading conditions [8, 9, 10, 11].

Yuen [8] and Wiehahn [9] analysed the capping of mild steel plates subjected to localised blast loading and identified shear type failure surfaces inclined at either 45° or 135° to the plates thickness direction. Numerical simulation of the blast tests captured two bands of high temperature material at the fracture location propagating through the thickness of the material at the same inclined angle of the experimental fracture surfaces. Bammann [10] studied the fracture of HY-100 and HY-130 steel under localised blast loading and stated the fracture and capping of the plates were caused by narrow bands of intense shear as the plastic deformation (in the plate) is converted to heat.

As part of a broader investigation into failure and rupture of materials under blast loading, Langdon et al. [11] compared the appearance of mild steel and high strength Armox 370T armour steel, ruptured under localised blast loading (Figure 1). The differences in the fracture mode of the two materials is evident. The mild steel exhibited a large thickness reduction around the fracture location and a fibrous surface appearance suggestive of tensile tearing. In contrast, the Armox 370T armour steel displayed minimal thickness reduction and an illustrious fracture surface inclined to the plate thickness, which is suggestive of brittle cracking failure mode.

Fig. 1. Target plates ruptured under localised blast loading [11]. Left, Mild steel with tensile fracture. Right, Armour steel with cracking fracture

In this investigation two armour grade steels intended for use in protective structures are studied. First is high hardness armour (HHA) steel commonly accepted as suitable for ballistic protection, and second is rolled homogenous armour (RHA) steel commonly accepted as suitable for blast protection. The response of each steel to localised blast loading was evaluated in terms of its maximum permanent displacement for a range of loading conditions and the charge mass required to rupture the plate. These tests provide new insight into the deformation resistance and energy absorption capability of these armour-grade materials. In addition, the tests examine the potential of HHA steel for blast protection applications.

2. Candidate Materials

The RHA material is specified as class 1 rolled homogeneous armour by MIL-DTL-12560 [12] and represents a common class of material used in armour systems for protection against blast loading. The HHA material is specified as high hardness armour by MIL-DTL-46100E [13] for protection primarily against ballistic threats. Key material properties including the specific energy to tensile fracture (SETF), given by the area under a uniaxial stress strain curve, are provided in Table 1. Characterization of each material under quasi-static tensile loading was conducted and reported by McDonald et al. [14]. Figure 2 provides a comparison between the stress–strain curves for each material.

Table 1. Candidate material class and mechanical properties considered in blast testing

Material	Yield Strength (MPa)	Elongation (%)	Charpy Impact Energy (J)	SETF (MJ/m^3)
RHA	1070	14.3	22	145
HHA	1200	12.3	16	177

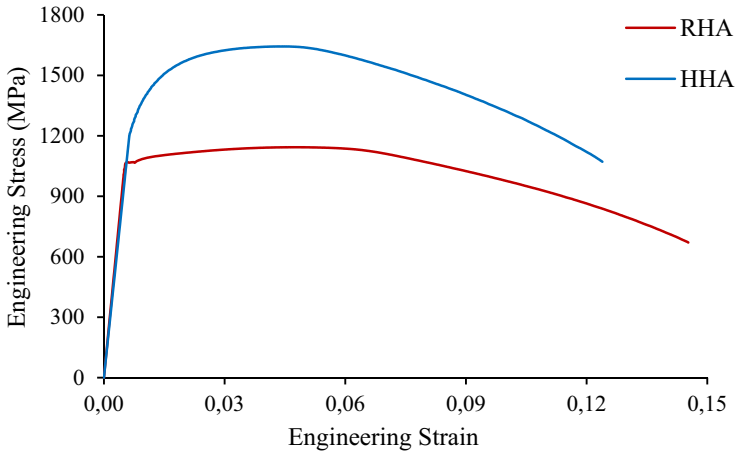

Fig. 2. Quasi-static stress vs. strain curves obtained for candidate materials

3. Experimental Arrangement

Blast testing was performed at the Blast Impact and Survivability Research Unit (BISRU) at the University of Cape Town with the test setup shown in Figure 3. Square test plates were fabricated for each of the candidate materials. Each plate had dimensions of 500 mm × 500 mm × 4 mm. The HHA material was provided by the manufacturer at the specified thickness whereas the RHA was wash ground to the correct thickness from a thicker plate (i.e. 6 mm). Hardness testing of the ground plates showed no significant change in the mechanical properties over the as received plates. The test plates were secured between two 20 mm thick clamping frames leaving an exposed area of 400 mm x 400 mm. The clamping frame was secured by 28 bolts tightened to at an average torque of 150 Nm. The test plates

were fixed to instrumented ballistic pendulum allowing the impulse imparted on the plate to be captured for each test. This ballistic pendulum test methodology has been used extensively by BISRU with further details provided by Nurick and Martin [15]. PE4 plastic explosive was formed into cylindrical charges with a fixed diameter of 50 mm. The mass of the charge was varied by altering its height to produce varying levels of blast loading. The charge was detonated at the centre of the rear face by an electric detonator. Polystyrene bridges were used to generate the stand-off distance (SOD) between the bottom of the explosive charge and the steel plate. The two SODs used throughout the test program were 25 mm and 13 mm.

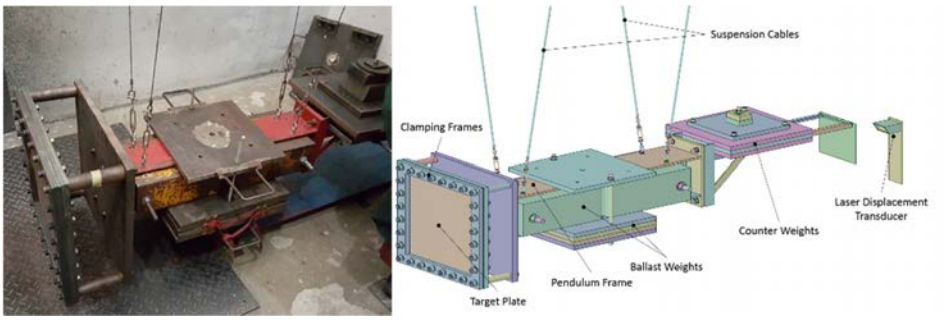

Fig. 3. Test plate clamped to instrumented ballistic pendulum

4. Blast Test Results

The primary objective of the experimental series was to isolate the charge mass rupture threshold of each candidate material at a SOD of 25 mm and 13 mm. Additional information on material response in Mode I and at charge sizes beyond the rupture threshold was also gathered throughout the series. The results from 30 blast tests are documented in Tables 2 and 3.

Table 2. Tabulated summary of the blast test results for RHA material

Test no.	Material	Stand-off distance (mm)	Charge diameter (mm)	Charge mass (g)	Impulse (Ns)	Permanent deflection (mm)
1	RHA	25	50	40	61.0	24.7
2	RHA	13	50	37.5	64.5	29.7
3	RHA	13	50	37.5	71.4	30.2
4	RHA	13	50	40	73.0	Torn
5	RHA	13	50	40	75.8	33.4
6	RHA	25	50	50	81.5	29.2
7	RHA	25	50	52.5	85.8	Torn
8	RHA	25	50	50	86.2	Torn
9	RHA	25	50	55	88.8	Torn
10	RHA	25	50	52.5	93.1	30.7
11	RHA	25	50	60	96.5	Torn
12	RHA	25	50	55	97.7	31.2
13	RHA	25	50	55	98.4	Torn
14	RHA	25	50	52.5	102.1	32.1
15	RHA	25	50	70	114.0	Torn

Table 3. Tabulated summary of the blast test results for HHA material

Test no.	Material	Stand-off distance (mm)	Charge diameter (mm)	Charge mass (g)	Impulse (Ns)	Permanent deflection (mm)
16	HHA	13	50	30	61.2	21.2
17	HHA	13	50	35	62.8	24.2
18	HHA	13	50	37.5	66.1	26.2
19	HHA	13	50	40	69.6	26.7
20	HHA	25	50	40	72.3	20.7
21	HHA	13	50	40	72.7	Torn
22	HHA	13	50	40	78.5	Torn
23	HHA	25	50	57.5	86.4	27.3
24	HHA	25	50	52.5	90.5	27.2
25	HHA	25	50	57.5	92.7	26.5
26	HHA	25	50	50	94.7	26.2
27	HHA	25	50	60	96.8	Torn
28	HHA	25	50	60	99.8	30.2
29	HHA	25	50	60	107.9	Torn
30	HHA	25	50	70	110.5	29.2

4.1. Deformation Performance

The Deformation resistance of the candidate materials can be compared at four loading conditions under which both materials were tested. A comparison of the permanent deformation for each material is given in Figure 4. The higher yield strength of the HHA steel reduces the deformation between 9% and 14% compared to the RHA steel for a given loading condition. With a similar magnitude of deformation reduction for blast loading at 13mm and 25mm stand-off distances, the improvements in deformation resistance did not appear to be dependent on the degree of localisation or proximity experienced during loading. These results confirm that the HHA steel provides better resistance to deformation than the RHA steel.

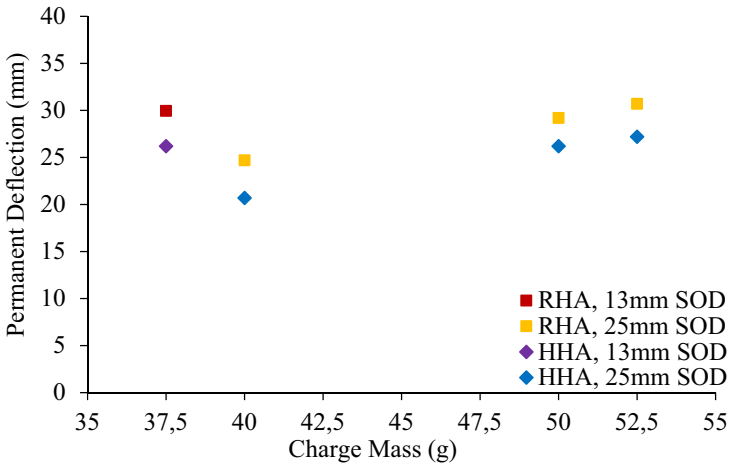

Fig. 4. Relative deformation resistance of candidate steels

4.2. Rupture Performance

As seen in Table 2, the charge mass to induce fracture for each material ranged across several grams. Hence, the rupture threshold is defined as the minimum charge mass at which 2/3 of tests produced a through thickness fracture. Table 3 documents the rupture threshold for each candidate material for both the 13 mm and 25 mm SODs. Whilst the HHA steel ruptured at 9% higher charge sizes than the RHA steel for the 25 mm SOD, both materials performed similarly at the 13 mm SOD. It is envisaged that the relative performance of the materials is due to the increased localisation of loading and higher strain rates at the lower SOD. The results confirm that HHA steel has the potential to be used in blast protection applications as it has a similar or better rupture performance at 13 mm and 25 mm SODs, respectively.

Table 4. Experimental rupture threshold of candidate materials for 13mm and 25mm SOD

Material	13mm SOD Rupture Threshold		25mm SOD Rupture Threshold	
	Charge mass (g)	Impulse (Ns)	Charge mass (g)	Impulse (Ns)
RHA	40.0	74.4	55.0	95.0
HHA	40.0	74.8	60.0	101.5

A promising correlation was identified by Langdon et al. [11] for the prediction of a materials rupture threshold from its specific energy to tensile fracture (SETF), which is given by the area under a uniaxial tensile stress-strain curve. Their experimental data for a range of materials including Armox 370T armour steel and two grades of mild steel showed a linear relation for all materials between their SETF and the non-dimensional impulse parameter at fracture given by equation 1 [7].

$$\phi_{ql} = \frac{I\left(1+\ln\left(\frac{LB}{\pi R_0^2}\right)\right)}{2t^2(LB\rho\sigma)^{\frac{1}{2}}} \tag{1}$$

Where, I is the impulse measure by the ballistic pendulum, R_0 is the explosive charge radius, L, B and t are the target plates dimensions, ρ is the target plates density and σ is the target plates yield strength.

Figure 5 compares the results from Langdon et al. [11] with the HHA and RHA steel used in this investigation in terms of their SETF and non-dimensional impulse parameter at rupture. While the RHA material appears to conform to the previous relation, the HHA is clearly rupturing at a magnitude of blast loading far lower than would be predicted by its energy absorption capability.

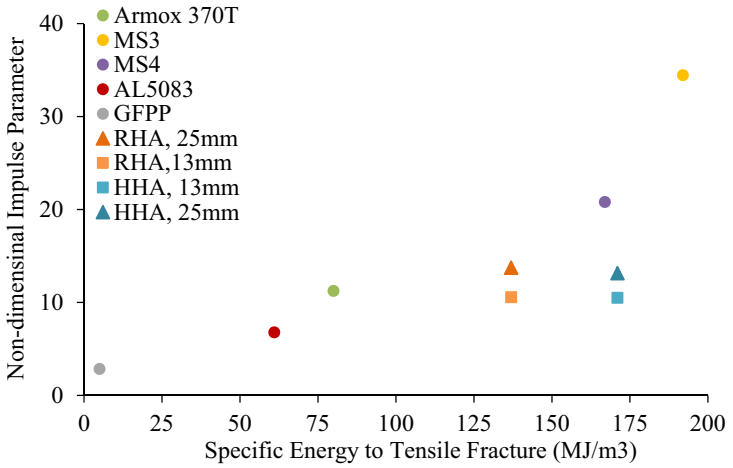

Fig. 5. Relation between non-dimensional impulse parameter and specific energy to tensile fracture for various materials

5. Fracture Modes

Optical examinations of the fractured plates showed a similar fracture initiation mode in both materials. Incomplete capping of the plate with little to no localised thickness reduction was generally observed at the first occurrence of fracture (Figure 6). At the rupture threshold, the crack initiation location was generally the mid-point of the un-separated cap and had an appearance distinct to the surrounding material. The fracture surface was highly inclined to the plate thickness direction and had a smooth appearance compared to the multiple opposing shear lips along the fracture surface. In contrast to the necking and tensile tearing observed in the testing of mild steels [5-7, 14], this suggests a shear-type failure mode is dominant in both armour grade materials. This shear-type failure mode may account for the poor correlation between rupture threshold and tensile energy absorption capability highlighted in section 4.2.

Fig. 6. Partial capping of candidate materials. Left: RHA, Right: HHA

In contrast to the development of a petalling failure mode, the post-rupture crack propagation of the RHA steel was minimal. The fracture pattern of RHA plates across a 20g range of charge masses in excess of the rupture threshold is shown in Figure 7. Beyond the progression from partial to full capping failure there is little change in the plate appearance.

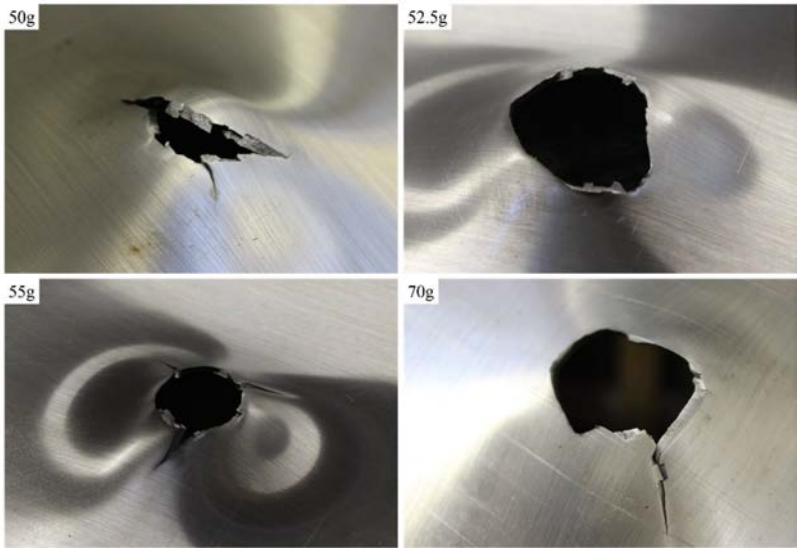

Fig. 7. Fracture pattern of RHA plates from initial rupture to 40% overmatched loading

In-line with its lower fracture toughness, the magnitude of radial crack propagation in the HHA steel was far higher and developed at the minimum charge to induce rupture. Figure 8 shows a crack generated by a 60g charge at a 25mm standoff distance (Tests no. 29). The surface appearance changes markedly along the length of the crack and gives insight into the fracture modes present at that location. The fracture initiation location at the apex of the petal appears smooth and is angled at approximately 45◦ to the plate's thickness. Several shear lips and a rough faceted surface characterises a region of mixed-mode crack propagation where circumferential and radial cracks are interacting. Proceeding down the crack, the surface shows signs of brittle crack propagation with chevrons aligned along the surface, the orientation of these ridges highlight that the crack has propagated radially ahead of the out-of-plane motion of the petal.

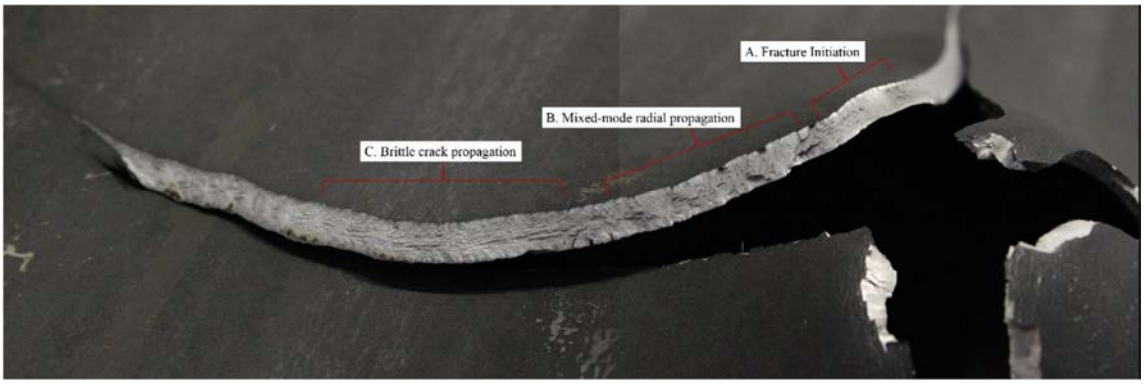

Fig. 8. Composite image of radially propagating crack in HHA steel plate showing transitions in fracture surface appearance

Optical and scanning electron microscopy was used to analyse the blast loaded plates and confirm the fracture mechanisms involved in initial rupture, capping and radial crack propagation. Inspection of fractured uniaxial tensile samples was also performed to highlight the expected appearance of a tensile and shear type fracture surface. Figure 9 compares the fracture surfaces of the HHA steel under uniaxial tension and localised blast loading. Elongated dimples and multiple ridged cracks on each surface show clear agreement between the tensile specimens shear lip and the slanted fracture surface of the blast loaded plate.

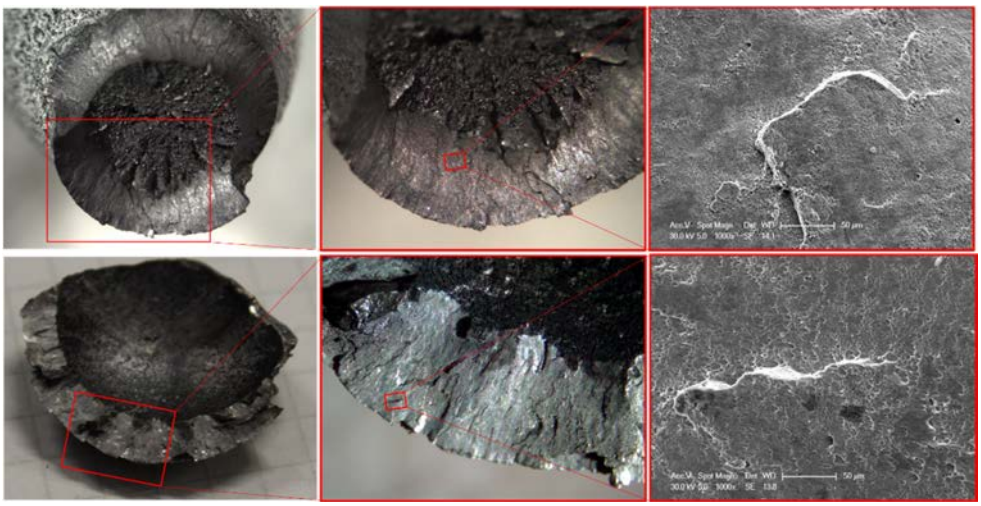

Fig.9. Fracture appearance of tensile sample and blast ejected cap for HHA steel showing shear fracture surfaces.

The shear fracture surface was confirmed on blast loaded samples for both candidate materials (Figure 10). In both cases the U-shaped dimples were orientated away from the fracture initiation edge of the unloaded face and point towards the plate centre.

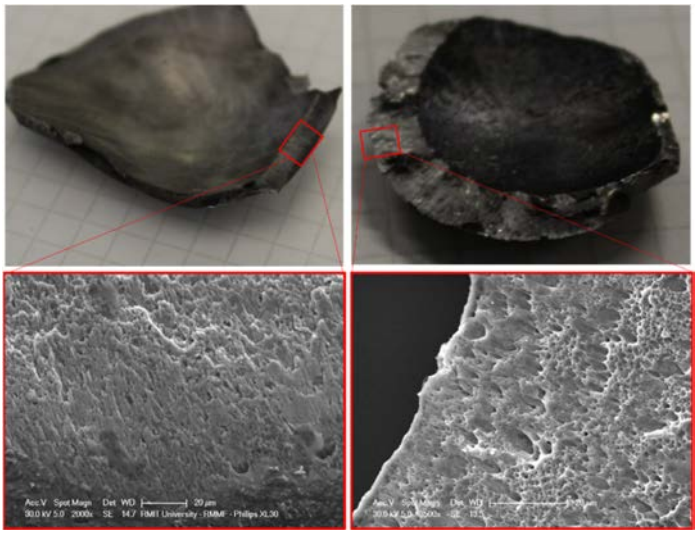

Fig.10. Fracture surfaces of ejected caps showing shear fracture modes across both candidate materials. Left: RHA, Right: HHA

6. Conclusions

The response of two armour grade steels to localised blast loading was experimentally evaluated in terms of deformation resistance and blast rupture threshold. The high hardness armour (HHA) steel was found to have reduced plate deformation compared to the rolled homogeneous armour (RHA) steel for a given magnitude of blast loading. Interestingly, the HHA steel, generally considered inappropriate for blast protection due to its limited ductility, also outperformed the RHA in terms of the charge mass required to fracture the plate at a stand-off distance (SOD) of 25 mm and provided identical performance to the RHA at a 13 mm SOD. The non-dimensional impulse at rupture for both materials was compared to previous data by Langdon et al. [11] and highlighted that the high hardness armour steel did not fit the established correlation between rupture threshold and specific energy to tensile fracture. Fractography was performed on the ruptured plates and confirmed a unique shear slant fracture mode dictating the energy absorption capability of these high strength materials under blast loading. Non-conformity of the high hardness armour steel to established theories of blast induced fracture highlights the need for more detailed predictive models accounting for the influence of shear-type failures on a materials rupture threshold under localised blast loading.

7. Acknowledgements

The authors acknowledge the support of the Defence Materials Technology Centre, which was established and is supported by the Australian Government's Defence Future Capability Technology Centre (DFCTC) initiative.

References

[1] Defence IQ. Global Armoured Vehicles Market Report 2016. Technical report, 2016.
[2] D F Haskell. Deformation and Fracture of Tank Bottom Hull Plates Subjected to Mine Blast. Technical report, 1972.
[3] C Choi, M Callaghan, and B Dixon. Blast Performance of Four Armour Materials. DSTO Technical report, 2013.
[4] W C Lee. An investigation of the response of different materials to blast loading. PhD thesis, University of Cape Town, 2012.

[5] G N Nurick and A M Radford. Deformation and tearing of clamped circular plates subjected to localised central blast loads. Recent developments in computational and applied mechanics: a volume in honour of John B. Martin: 276–301, 1997.
[6] V H Balden and G N Nurick. Numerical simulation of the post-failure motion of steel plates subjected to blast loading. International Journal of Impact Engineering, 32(1):14–34, 2005.
[7] N Jacob, S C K Yuen, G N Nurick, D Bonorchis, S A Desai, and D Tait. Scaling aspects of quadrangular plates subjected to localised blast loads- experiments and predictions. International Journal of Impact Engineering, 30(8):1179–1208, 2004.
[8] S C K Yuen, G. N. Nurick. The significance of the thickness of a plate when subjected to localised blast loads. In Proc 16th Int Symp Military Aspects of Blast and Shock: 491-499. 2000.
[9] Miles Alexander Wiehahn. Circular plates subjected to localised blast loads: some insights into the mechanism of tearing and the energy required. M.S thesis, University of Cape Town, 2000.
[10] D J Bammann, M L Chiesa, M F Horstemeyer, and L I Weingarten. Failure in ductile materials using finite element methods. Structural crashworthiness and failure: 1–54, 1993.
[11] G S Langdon, W C Lee, and L A Louca. The influence of material type on the response of plates to air-blast loading. International Journal of Impact Engineering, 78:150–160, 2015.
[12] U.S Detail Specification. MIL-DTL-12560K(MR), Armor Plate, Steel, Wrought, Homogeneous (For use in Combat-Vehicles and for Ammunition Testing), 2013.
[13] U.S Detail Specification. MIL-DTL-46100E(MR). Armor Plate, Steel, Wrought, High-Hardness, 2008.
[14] B McDonald, H Bornstein, and A Orifici. Characterisation of Armour Properties for the Prediction of Rupture in Localised Blast Loading. International Symposium for Ballistics, Edinburgh, 1: 1135-1146, 2016.
[15] G N Nurick and J B Martin. Deformation of thin plates subjected to impulsive loading- a review Part II: experimental studies. International Journal of Impact Engineering, 8(2):171–186, 1989.
[16] R G Teeling-Smith and G N Nurick. The deformation and tearing of thin circular plates subjected to impulsive loads. International Journal of Impact Engineering, 11(1):77–91, 1991.